Bridging by End-Adsorbed Triblock Copolymers

Mai Nguyen-Misra, Sanjay Misra, and Wayne L. Mattice*

Institute of Polymer Science, The University of Akron, Akron, Ohio 44325-3909

Received June 7, 1995; Revised Manuscript Received November 14, 1995⊗

ABSTRACT: In this Monte Carlo study, on a cubic lattice, we examine adsorption and bridging by ABA triblock copolymer chains confined between two parallel flat surfaces. The solvent is assumed to be athermal for both blocks and the only relevant energy parameter is ϵ_{AS}, the binding energy between the A segments and the surfaces. We study the role of the binding energy and the end block size (N_A) on the fraction of bridging chains. The bridging fraction and the fraction of adsorbing segments both depend explicitly on ϵ_{AS} and N_A, and not on the product $2\epsilon_{AS}N_A$ (which is the maximum available adsorption energy per chain). The dynamic response of the system to step and sinusoidal shear is examined. For $N_A = 1$, the system essentially behaves as a single Maxwell element. As N_A increases, the stress relaxation becomes increasingly nonexponential with a pronounced tail (due to a spectrum of relaxation times associated with the transient bridging). As for the storage and loss moduli, the limiting slopes ($\omega \rightarrow 0$) of log G' vs log ω G'' vs log ω go from 2 to 1 and 1 to 0.5, respectively, as N_A goes from 1 to $N_A \gg 1$.

1. Introduction

It is well established that the structure of the adsorbed polymer layer at the solid/fluid interface dominates the interaction between such interfaces.[1] The interaction, for adsorbing homopolymers (a complicated system), is purely attractive at long range and becomes repulsive at shorter ranges. For polymer brushes, tethered the surface only at one end (a simple system), the interaction is purely repulsive.[1−6] Polymers containing adsorbing sites[2,4−10] at both ends can produce the complex behavior exhibited by adsorbing homopolymers and yet have the simpler underlying physics that characterizes end-grafted systems. The interaction may change from repulsive to attractive, depending on the conformations of the chains. When both ends adsorb on the same surface (loop conformation), the interaction between two such adsorbed layers is repulsive, similar to the interaction between two adsorbed layers of polymers with one adsorbing end. Under certain conditions, the end blocks may adsorb on different surfaces, bridging the two surfaces; the bridging induces attraction between the two surfaces, which competes with the repulsive interaction characteristic of two opposing brushes.[8,9] Homopolymers have been used for many years as stabilizers and flocculants.[1] However, due to the complexity of the adsorption behavior, the stability of the colloidal suspensions is not well controlled. Triblock copolymers therefore represent a model avenue to affect the colloidal stability and rheology of a suspension, the added advantage being the simple underlying physics that makes them more amenable to rational design to suit a particular application.

The phase stability of a colloidal suspension can be altered by suitable tailoring of triblock copolymer chains. By varying the colloidal particle concentration (distance between surfaces), adsorption energy, degree of polymerization, the solvent quality, and polymer concentration, one can control the degree of bridging and thus the nature of the interaction (purely repulsive when no bridging occurs to long-range attractive with some bridging). Indeed many of the recent studies, both experimental[4,5] and theoretical (using either the self-consistent mean field theory[7−9] or a Monte Carlo technique[10]), on triblock chains, tethered by both ends to surfaces, have focused on the bridging attraction aspect.

Weakly adsorbing polymer chains can also form transient networks, whose dynamic response is not well understood at the molecular level. Transient networks formed by end-adsorbing triblock copolymers on surfaces may also serve as a model network. This system, while providing a model for studying transient networks, in general, differs in some respects from transient networks formed by self-association of triblock copolymer chains. The adsorbing systems have a far greater functionality; their compression and expansion are asymmetric and the shear and longitudinal moduli are no longer proportional to one another. In addition, the bridging distance is an input for the adsorbing problem, whereas in self-associating systems the bridging distance is determined by the density of the micelles. The complexity of the self-associated systems is thus removed in the case of adsorbing triblock copolymers.

Theories on the dynamic aspects of transient networks were initially developed to explain the stress decay in viscoelastic polymeric systems.[12−14] More recently, Tanaka and Edwards (TE)[15−18] and Wang[19] addressed the time evolution of stress after a step strain had been applied to the network in the unentangled regime. The system considered by TE and Wang was a melt of monodisperse chains, with each chain having one sticky group at each end—the self-association leading to a transient network.

One theoretical model that applies to the simulations reported in this study is due to Baxandall. Baxandall's model examines the motion of a chain with sites that bind reversibly with a phantom network (i.e., absence of tubelike confinement effects), which itself had permanent cross-links.[20] In general, the length of the subchains between cross-links is variable with a spectrum of relaxation times associated with each subchain. This is a refinement over the simple theory of Lodge,[13] which assumed only one relaxation mode for each subchain between cross-links. For chains with cross-links only at the two ends under a step strain, a time-evolution relaxation modulus exhibiting a single relaxation rate was found. As the number of cross-links increased the relaxation of adjacent segments became correlated, resulting in slower relaxation.

Another set of theories, including the Gonzalez[21,22] and Leibler, Rubinstein, and Colby[23] (LRC) models,

⊗ Abstract published in *Advance ACS Abstracts,* February 1, 1996.

examined the relaxation of a chain with sites that bind reversibly with a host network, with entanglement effects incorporated. The diffusion of a networked chain is modeled using the reptation model of Doi and Edwards.[24] The LRC model would be relevant when the density of adsorbed triblock layers is large and when the polymer chains are very long—leading to entanglement effects.

In section 2 the ranges of parameters employed in the simulations are presented as are the details on how the equilibrium ensembles of chains were generated and how the dynamics of the chains was followed. The variable parameters in this study are the number of segments in the end block (N_A) and the energy of interaction between the end block segments and the surfaces ($\beta\epsilon_{AS}$). The effects of surface separation were explored previously.[29] The equilibrium properties of the system, namely the chain populations, the segment density profile, the fraction of A segments adsorbed, and the bound number of segments per adsorbed A block, are presented in the first part of section 3. In part 2, the results of the chain dynamics, with focus on the effects of N_A and $\beta\epsilon_{AS}$ not only on the average lifetimes of the bridges but also on the distribution of lifetimes, are examined. The bridge lifetime distributions are used to predict the shear stress relaxation modulus for the system in the linear response regime (part 3). In part 4 of section 3, the effects of $\beta\epsilon_{AS}$ and N_A on the dynamic moduli are discussed. The main results are summarized in the last section, section 4.

2. Simulations

2.1. System Variables. The simulations were carried out on a cubic lattice with periodic boundary conditions in the x and y directions. The lateral dimensions of the lattice box, x and y, were fixed at 30 lattice units. Two impenetrable adsorbing surfaces were placed at $z = 0$ and $(D + 1)$, respectively. The number of sites accessible to a bead in the periodic box was $30 \times 30 \times D$. The simulation was performed at various separations of the two surfaces, ranging from 9 to 21 lattice units. The majority of the runs were carried out at an intermediate value of D ($D = 11$). These values of D were chosen for two main reasons: (1) The bridges were not stretched more than twice the root-mean-square end-to-end distance of a free chain (under which conditions, chain stretch has been shown to have negligible influence on chain dynamics[29]). The dimensionless root-mean-square end-to-end distances, $\langle r^2\rangle^{1/2}$, range from 9 to 13 lattice units for chains with N ranging from 40 to 70. (2) There were enough bridging events to obtain good statistics. A two-dimensional representation of three states of end-adsorbed triblock copolymers confined between two surfaces is illustrated in Figure 1.

All simulations were performed with 20 chains of equal chain length N, where N is $(2N_A + N_B)$. This choice of M, where M is the number of chains in the system, gave a grafting density of 0.022 chains per site. The symmetric ABA triblock copolymers were constructed as self-avoiding walks on a cubic lattice. The A blocks were the adsorbing blocks; i.e., the interaction between the A segments and the surface was attractive or $\epsilon_{AS} < 0$. The values of end block size N_A studied were 1, 5, 10, and 15 while the number of segments in the middle block N_B was usually fixed at 40. For the values of D chosen, the range of concentration studied (~0.06–0.14) fell below or in the range of the overlap concentrations (~0.11–0.20). At this range of concentration,

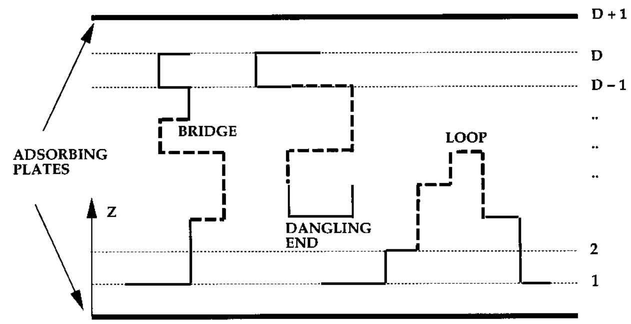

Figure 1. A two-dimensional representation of three states of end-adsorbed ABA triblock copolymers confined between two surfaces. The solid and dashed lines represent the A and B segments, respectively.

interchain interactions play a negligible role in defining the chain conformations.[10] The isolated adsorbed layer heights (e.g., when the two adsorbing plates are far apart from one another) are of the same order of magnitude as $\langle r^2\rangle^{1/2}$ of free chains.[10]

The solvent was taken to be athermal to exclude any self-association. The only nonzero energy term in the simulation was the binding (adsorption) energy, $\beta\epsilon_{AS}$, where $\beta = 1/kT$, between the end block segments and the adsorbing surfaces. The end block size effects were studied under two scenarios: (i) constant total available adsorption energy per chain, $2\beta\epsilon_{AS}N_A$, while both N_A and $\beta\epsilon_{AS}$ were varied and (ii) constant $\beta\epsilon_{AS}$ while N_A (and hence $2\beta\epsilon_{AS}N_A$, the maximum available adsorption energy) was varied. For case i, the values of $-2\beta\epsilon_{AS}N_A$ investigated were 2, 4, and 6. Case ii was studied for $-\beta\epsilon_{AS} = 0.4$, 1.0, and 2.0. In this range of adsorption energies, the adsorption was reversible.[10]

The effects of binding energy, $\beta\epsilon_{AS}$ (ranging from -0.1 to -2.0), were explored using $N_A = 5$ or 10, $D = 11$, and $N_B = 40$. A separate set of simulations, focusing on the effects of binding energy on the dynamics of systems of triblock copolymer chains with $N_A = 1$, was performed for various values of D, ranging from 11 to 21 lattice units, and $N_B = 48$. These simulations were performed with $-\beta\epsilon_{AS} = 1$, 2, 3, and 5 for each value of D.

2.2. Simulation Details. The procedures for generating the equilibrium configurations and dynamics trajectories were described in earlier works.[10,29] After the relaxation process, where initial chain conformations were generated, the energy between the chain ends and the surfaces, $\beta\epsilon_{AS}$, was turned on and 10 million moves were attempted in order to attain equilibrium. The chain segment density distributions were calculated and averaged over 200 configurations, chosen at regular intervals from the last 3 million moves of a given trajectory.

The final equilibrium configuration was used as the initial configuration of the dynamics trajectory. In each dynamic run, the state of each chain and the number of segments adsorbed (ranging from 0 to N_A) for each A block were stored at every Monte Carlo time step (1 Monte Carlo time step = $N \times M$ attempted moves) for 5000 Monte Carlo time steps. The chain fraction (free, dangling, loops, and bridges), fraction of A segments adsorbed (θ_a), number of A segments adsorbed per adsorbing A block (n_a), and lifetime spectrum of bridges ($P(\tau)$) were extracted from the dynamics trajectories. The average bridging lifetime, $\langle\tau_B\rangle$, is calculated using $P(\tau)$.[29] It is expected that the uncertainty in $\langle\tau_B\rangle$ increases as either the binding energy or N_A increases.

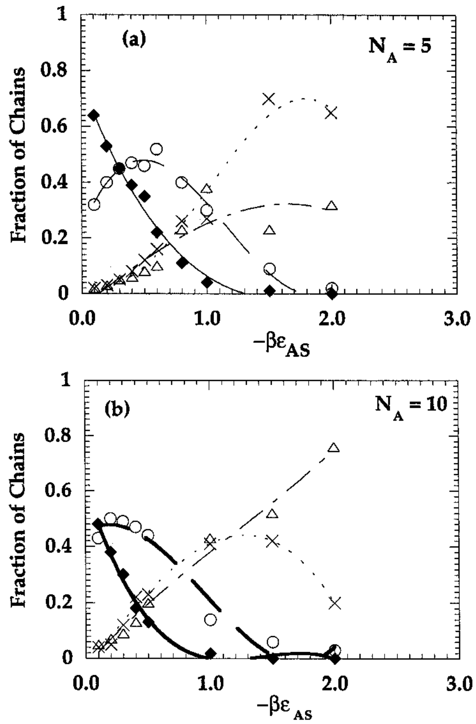

Figure 2. Fraction of chains present as (◆) free chains, (○) dangling ends, (×) loops, and (△) bridges as a function of $-\beta\epsilon_{AS}$ when $N_B = 40$, $D = 11$, and N_A is (a) 5 and (b) 10.

Error analysis (on $\langle\tau_B\rangle$) was performed on simulations with high binding energies, $-2\beta\epsilon_{AS}N_A > 10$. To estimate the average value of $\langle\tau_B\rangle$ and its corresponding standard deviations, a series of 5 runs for selective sets of $\{-\beta\epsilon_{AS}, N_A\}$ was carried out.[30] The time-dependent relaxation modulus $G(t)$ and shear stress $\sigma(t)$ were predicted using the bridging lifetime distribution, $P(\tau)$. Subsequently, the complex modulus was obtained using $G(t)$.

3. Results and Discussion

3.1. Equilibrium Properties. The segment density profiles for various values of N_A are typical of end-adsorbed polymers, showing a steep entropic depletion near the surface and increasing to a maximum value at short distance from the surface. Because of the small surface separation, extensive penetration of one adsorbing layer into the other is observed.

In panels a and b of Figure 2, the dependencies of fraction of the chains in each of the four states on $\beta\epsilon_{AS}$ are illustrated for two different values of N_A. In general, as the binding energy increases, more free chains and dangling ends are converted to bridges and loops, until finally all chains occupy only those two states. These trends occur at smaller $-\beta\epsilon_{AS}$ for those chains with longer end block size, due to their higher total available adsorption energy. As $-\beta\epsilon_{AS}$ increases, it becomes energetically more favorable for the dangling ends and free chains to trade in the translational freedom of the free ends by adsorbing at both ends. As $-\beta\epsilon_{AS}$ increases, the concentration of free chains decreases monotonically while the concentration of dangling ends passes through a maximum at intermediate $\beta\epsilon_{AS}$ (panels a and b of Figure 2). The concentrations of bridges and loops increase steadily with increasing $-\beta\epsilon_{AS}$ at low-to-intermediate range of $-\beta\epsilon_{AS}$.

Similarly, panels a and b of Figure 3 show that both the fraction of A segments adsorbed, θ_a, and the number of bound A segments per adsorbed A block, n_a, increase

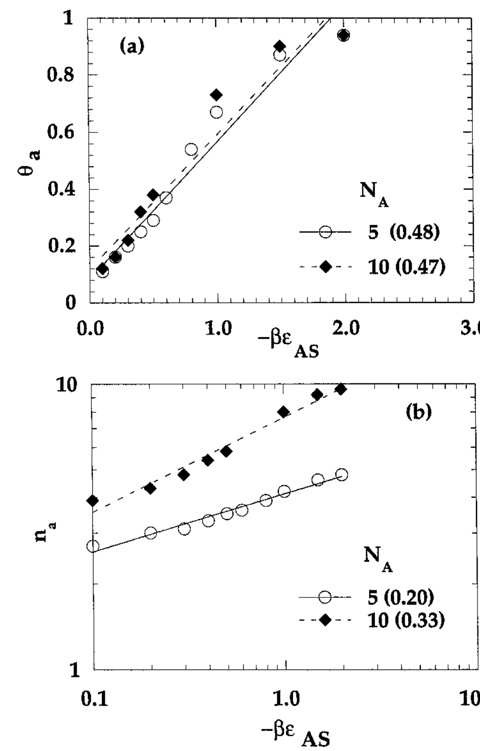

Figure 3. Effects of binding energy on (a) θ_a and (b) n_a when $N_B = 40$, $D = 11$, and N_A is 5 or 10. The lines are the best linear (a) and power-law (b) fits to the data. The numbers in parentheses are the slopes of the lines.

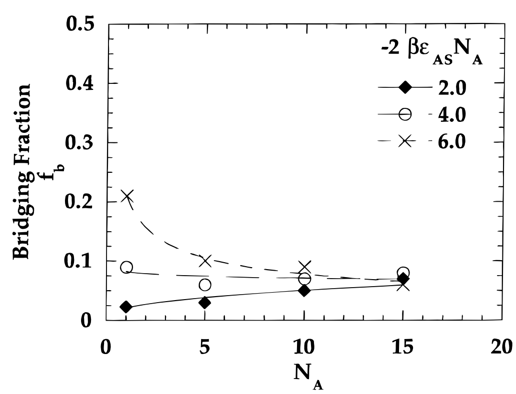

Figure 4. Effects of end block size on bridging fraction when $-2\beta\epsilon_{AS}N_A =$ (◆) 2.0, (○) 4.0, and (×) 6.0, with $D = 11$ and $N_B = 40$.

as $-\beta\epsilon_{AS}$ increases. These results have important consequences on the lifetimes of bridges, as will be discussed in part 2 of this section.

The effects of N_A on the population of bridges are illustrated in Figure 4 for various values of $-2N_A\beta\epsilon_{AS}$. Our results show that in the weak adsorption regime, when the energetic benefit is not sufficient to overcome the entropic loss from adsorption, it is entropically more favorable for chain ends to remain free. The bridging fraction is small and constant at $-2N_A\beta\epsilon_{AS} = 4$ but decreases with increasing N_A at slightly higher $-2N_A\beta\epsilon_{AS}$. The decrease in bridging fraction may explain the observation of Wijmans et al. that repulsion increases as N_A increases for a constant $2N_A\beta\epsilon_{AS}$.[9] In panels a and b of Figure 5, θ_a and n_a are examined, respectively. Panel a shows that θ_a decreases as N_A increases. In panel b, n_a increases, in a power-law fashion, as N_A increases. These observations suggest, as also illustrated by Wijmans et al.,[9] that changing either N_A or $\beta\epsilon_{AS}$ by the same factor does not produce equivalent

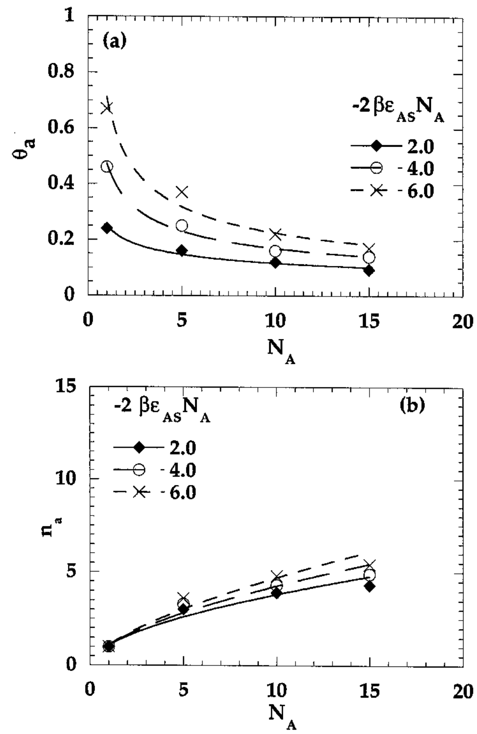

Figure 5. Effects of end block size on (a) θ_a and (b) n_a when $-2\beta\epsilon_{AS}N_A$ = (◆) 2.0, (○) 4.0, and (×) 6.0, with $D = 11$ and $N_B = 40$.

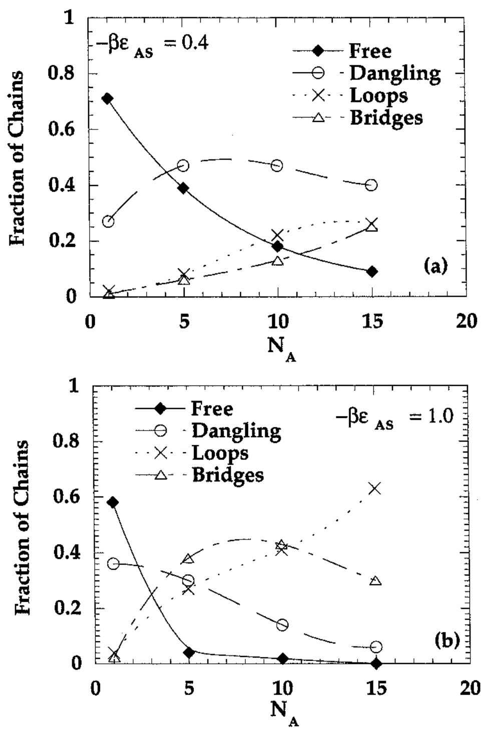

Figure 6. Fraction of chains present as (◆) free chains, (○) dangling ends, (×) loops, and (△) bridges as a function of N_A when $N_B = 40$, $D = 11$, and $-\beta\epsilon_{AS}$ is (a) 0.4 and (b) 1.0.

effects. In other words, f_b, θ_a, and n_a are explicit functions of $\beta\epsilon_{AS}$ and N_A, not of the product $2N_A\beta\epsilon_{AS}$. Adsorption behavior with $N_A = 10$ and $-\beta\epsilon_{AS} = 0.1$ is not duplicated by adsorption behavior with $N_A = 5$ and $-\beta\epsilon_{AS} = 0.2$.

Since experimentalists often change N_A, we examine in panels a and b of Figure 6 the chain fraction as a function of N_A for $-\beta\epsilon_{AS} = 0.4$ and 1.0, respectively. At low $-\beta\epsilon_{AS}$, the concentrations of free chains, loops, and bridges are monotonic functions of N_A, but the concentration of dangling chains passes through a broad maximum. At small N_A, or low $-2N_A\beta\epsilon_{AS}$, when the entropic effects are more important, free chains are converted to bridges and loops, as well as to dangling ends. At high N_A, when energetic effects are important, those dangling ends along with the free chains convert to bridges and loops as N_A increases. In Figure 7, n_a is seen to increase as N_A increases. Our results also show that the fraction of A segments adsorbed increases with increasing N_A.

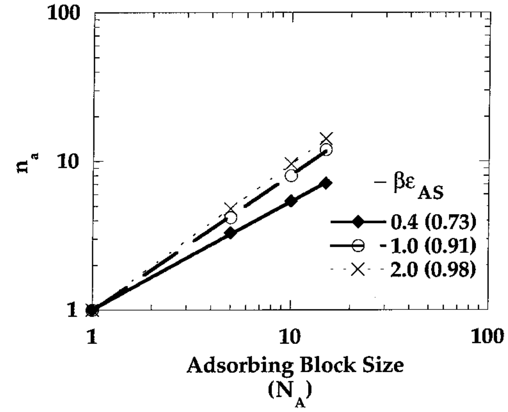

Figure 7. n_a as a function of N_A for $N_B = 40$, $D = 11$, and $-\beta\epsilon_{AS}$ = 0.4 (◆), 1.0 (○), and 2.0 (×). The lines are the best power-law fits to the data. The numbers in parentheses are the slopes of the lines.

3.2. Bridging Lifetime Distributions. How the bridging lifetime distribution may be deduced from the history of states has been discussed elsewhere.[29] In this section, we will show that the probability density of bridges with a given lifetime τ, $P(\tau)$, can be fitted to a single exponential decay function only when $N_A = 1$. In other words, for triblock copolymer chains having $N_A = 1$, $P(\tau) \sim \exp(-\tau/\tau_c)$, where τ_c is the characteristic time. For $N_A > 1$, the distribution function is no longer exponential. Our data seem to suggest that $P(\tau)$ may be a complex sum of several exponentials, each with its own characteristic lifetime, when $N_A > 1$.

In panel a of Figure 8, the normalized probability density, $P(\tau)$, of finding a bridge with lifetime τ is shown for different energies for $N_A = 1$, $N_B = 48$, and $D = 11$. Panel a illustrates that it is possible to fit the lifetime distribution to a single exponential decay, in accordance with the dumbbell model of Baxandall (corresponding to the relaxation of a telechelic chain in a phantom host network). Similar fits can be obtained for $D = 14$ and 16, although for larger values of D there are fewer bridging events and the fits, consequently, have higher uncertainties. As expected, the decay occurs on longer time scales as the binding energy increases.

The average bridging lifetimes, $\langle\tau_B\rangle$, are shown as a function of $-\beta\epsilon_{AS}$ for $N_A = 1$ and various values of D in panel b of Figure 8. For D = 11, 14, and 16 (i.e., bridges that are stretched not more than twice $\langle r^2\rangle^{1/2}$ of a free chain of $N = 50$, 9.04), $\langle\tau_B\rangle$ increases exponentially with the binding energy. In other words,

$$\langle\tau_B\rangle \sim e^{-\beta\epsilon_{AS}} \tag{1}$$

However, for higher stretching, or D = 19 and 21, the elastic energy also plays a role in the breaking of the bridges. The elastic energy stored in the stretched bridges cause them to break off sooner than compared to less stretched bridges of the same binding energy.

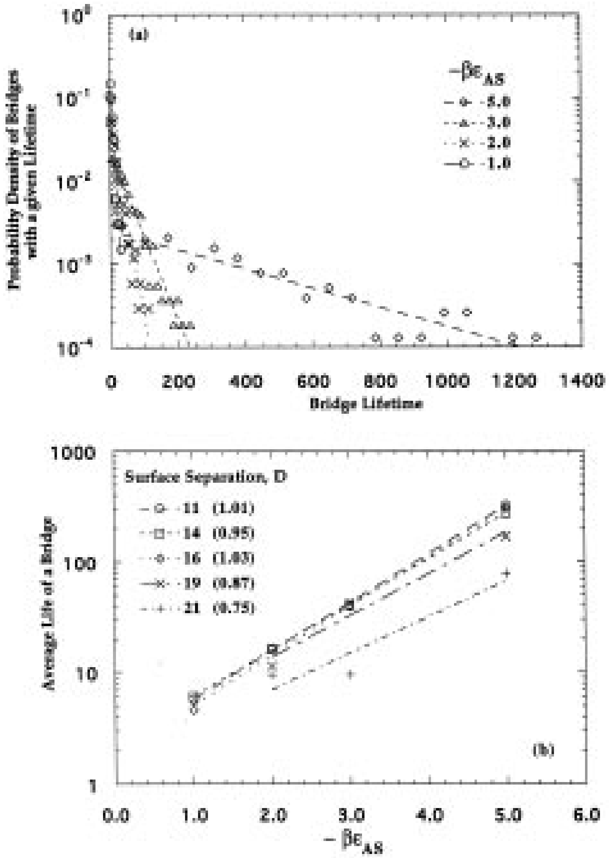

Figure 8. (a) Normalized probability density, $P(\tau)$, of a bridge with a given lifetime τ for $N_A = 1$, $N_B = 48$, $D = 11$, and various values of $-\beta\epsilon_{AS}$. The lines are the best exponential fits to the data. (b) Average bridging lifetime, $\langle\tau_B\rangle$, as a function of the binding energy, $-\beta\epsilon_{AS}$, for $N_A = 1$ and $N_B = 48$ with various values of surface separation. The lines are the best exponential fits to the data (the numbers in parentheses are the slopes of the lines).

The effects of surface separation on bridging lifetimes were discussed in detail in another study.[29]

Panel a of Figure 9 shows the probability distributions for various values of N_A when the binding energy is kept constant. This plot shows that $P(\tau)$ fits an exponential decay function when $N_A = 1$ but deviates from a simple exponential decay for $N_A > 1$. The decay appears more nonexponential and extends to longer lifetime as N_A increases. The distribution may be a combination of several exponentials, each with a different characteristic lifetime. In the breaking of a bridging end, there are a number of steps in which the adsorbed n_a segments could desorb; the number of segments involved in each desorption step is different, generating a spectrum of desorption times. As N_A increases, n_a increases and thus the distribution becomes more nonexponential and extends to longer lifetime.

Figure 9b illustrates the effects of N_A on $\langle\tau_B\rangle$ for various values of $-\beta\epsilon_{AS}$. As N_A increases, $\langle\tau_B\rangle$ increases, increasing at a faster rate for higher energies. As either N_A or $-\beta\epsilon_{AS}$ increases, both θ_a and n_a increase, resulting in larger contributions of longer lifetime modes. The lines in panel b are the best power-law fit to the data. The slopes of the lines are shown in parentheses.

The lifetime distributions (for $N_A = 5$ and $D = 11$) and $\langle\tau_B\rangle$ (for various values of N_A) are depicted in Figures 10 and 11, respectively, as a function of $-\beta\epsilon_{AS}$. The curves in Figure 10, using power-law fits, are drawn as visual guides. The distribution becomes more nonexponential and extends to longer lifetime as $-\beta\epsilon_{AS}$

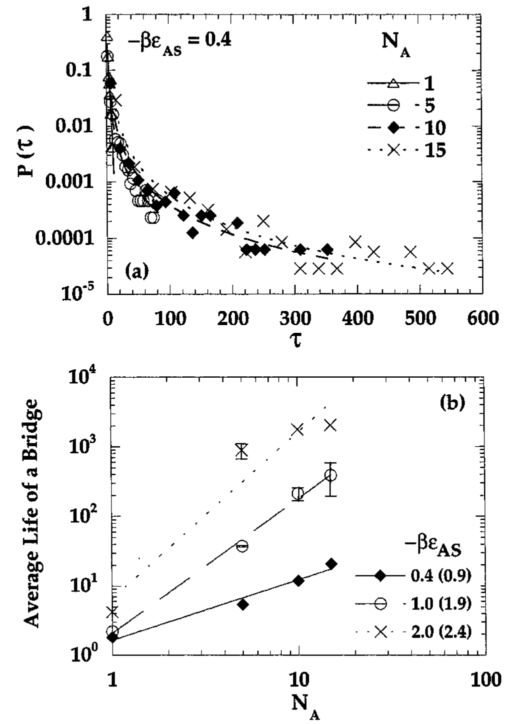

Figure 9. (a) $P(\tau)$ versus τ for $-\beta\epsilon_{AS} = 0.4$, $D = 11$, $N_B = 40$, and various values of N_A. Except for $N_A = 1$, the lines are drawn as visual guides. (b) Average bridging lifetime, $\langle\tau_B\rangle$, as a function of N_A for various values of $-\beta\epsilon_{AS}$.

increases. In addition, the contributions of the longer lifetime modes increase as $-\beta\epsilon_{AS}$ increases. In panel a of Figure 11, the average bridging lifetime, $\langle\tau_B\rangle$, is shown as a function $-\beta\epsilon_{AS}$ for $N_A = 5$ and 10. This figure shows that $\langle\tau_B\rangle$ still exhibits a simple exponential dependence on $-\beta\epsilon_{AS}$, as observed for the case of telechelic chains with $N_A = 1$. As $-\beta\epsilon_{AS}$ increases, not only n_a increases but the bound segments are also held more strongly, leading to an increase in $\langle\tau_B\rangle$. Importantly, panel b of Figure 11 illustrates that $\langle\tau_B\rangle$ depends on the effective adsorption energy ($\theta_a \times -2\beta\epsilon_{AS}N_A$) rather than the total available binding energy, $-2\beta\epsilon_{AS}N_A$.

3.3. Stress Relaxation after a Step Strain. The consequences of bridging lifetime distributions on the shear stress relaxation after one of the surfaces is sheared with respect to the other were also discussed in ref 29. There, the assumptions used in the analysis were also presented. Equations 2 and 4, respectively, are used to determine the time-evolution shear stress, $\sigma(t)$, and the stress relaxation modulus, $G(t)$.

$$\frac{\sigma(t)}{\sigma_0} = \sum_{\tau_i > t}^{\tau_{max}} P(\tau_i)\Delta\tau \tag{2}$$

$$\sigma_0 = (f_b \Xi \gamma)kT \tag{3}$$

$$\frac{G(t)}{kT} = f_b \Xi \sum_{\tau_i > t}^{\tau_{max}} P(\tau_i)\Delta\tau \tag{4}$$

In the present simulations with 20 chains and a surface area of 30 × 30, we have $\Xi = 20/900 = 0.022$, where Ξ^{-1} is the area available on either surface per chain. It is important to note that since the equilibrium bridging fraction, f_b, is a function of the system variables, the relaxation modulus depends upon the system parameters through both the relaxation time and the zero-time stress (eq 3) in the system.

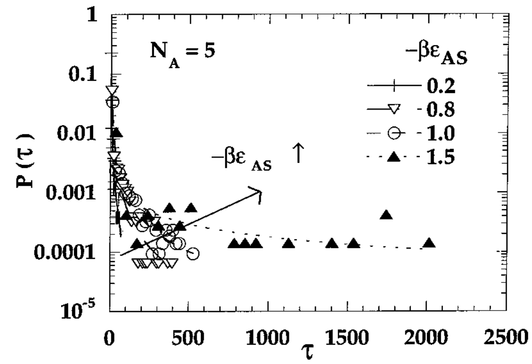

Figure 10. $P(\tau)$ versus τ for $N_A = 5$, $N_B = 40$, $D = 11$, and various values of $-\beta\epsilon_{AS}$. The lines are drawn as visual guides.

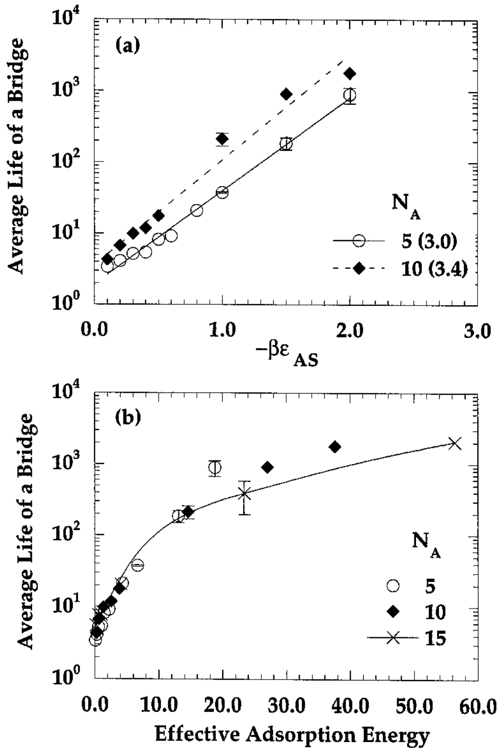

Figure 11. Average bridging lifetime, $\langle\tau_B\rangle$, as a function of (a) $-\beta\epsilon_{AS}$ and (b) effective adsorption energy, $(-2\beta\epsilon_{AS}N_A)\theta_a$, for $N_B = 40$, $D = 11$, and various values of N_A.

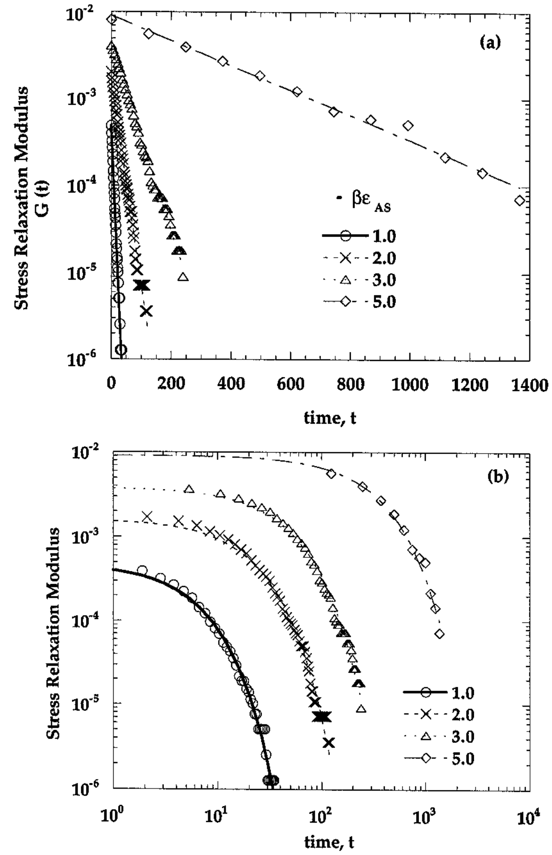

Figure 12. Time-dependent stress relaxation moduli shown on a (a) semi log and (b) log–log scale for $N_A = 1$, $N_B = 48$, and $D = 11$. The lines are the best exponential fits.

In the next two figures, we will show the viscoelastic response of various systems of triblock copolymer chains with $N_A = 1$ and $N_B = 48$. Given that $P(\tau) \sim \exp(-\tau/\tau_c)$ when $N_A = 1$, one would also expect an exponential decay for the modulus of such systems. In panels a and b of Figure 12, the time-dependent stress relaxation moduli for systems of telechelic chains are shown for various values of the binding energy at a given surface separation ($D = 11$). For each set of parameters, the time τ_{max} was divided into n equal time intervals such that, on average, 10 bridging events were observed for each time interval. The fractional stress remaining at the end of a given time interval was just the fraction of bridging events that were of larger lifetimes according to eq 2.

The data in panel a of Figure 12 are shown on a semilog arithmic plot along with a single exponential fit to each data set. Indeed a single exponential decay represents the stress relaxation very well, in good agreement not only with the model of Baxandall[20] for a dumbbell (a Rouse chain with two beads connected by a single spring) inside a phantom network but also with experimental observations of various solutions of associative thickeners.[31] Thus the viscoelastic response of a system of telechelic chains with $N_A = 1$ can be characterized by a single relaxation process and is therefore well represented by a single Maxwell element (a simple viscoelastic model consists of an elastic component, a spring, connected in series with a viscous component, a dashpot[32,33]). As expected from the bridge lifetime distributions, the stress decays on a slower time scale as the binding energy increases. Panel b of Figure 12 depicts the same data on a log–log plot and shows clearly that the time at which the plateau modulus decays and the system starts to flow is a strong function of the binding energy. The absolute value of the plateau modulus increases with increasing binding energy as well. The rubbery plateau region increases in width as the binding energy increases, indicating broadening of the relaxation time distributions.

Panel a of Figure 13, which depicts the time-dependence stress relaxation for various values of N_A, shows that the relaxation deviates from a simple exponential decay as N_A increases. Similar to the relaxation of end-associated triblock copolymers, the viscoelastic response of end-adsorbed triblock copolymers also appears to fit a stretched-exponential expression (panel b of Figure 13). However, it is believed that the relaxation is a sum of several exponentials rather than a stretched exponential, since there are no topological hindrances under the conditions investigated. However, it is impossible to resolve the response into individual exponentials, since the number of exponentials involved increases as N_A increases.

Figure 14 shows the time-dependent stress, on a semilog arithmic plot, for various values of binding

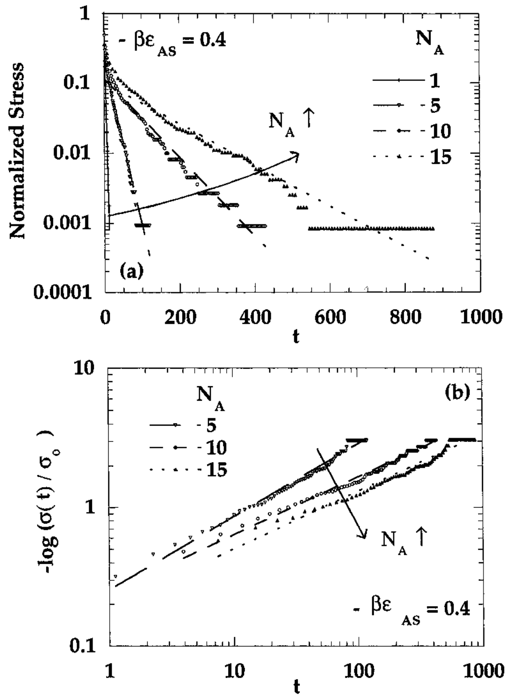

Figure 13. Normalized stress relaxation moduli for $N_B = 40$, $D = 11$, and various values of N_A as (a) $\sigma(t)/\sigma_0$ vs t, in a semilog plot and (b) $\log\{\sigma(t)/\sigma_0\}$ vs t in a log−log plot.

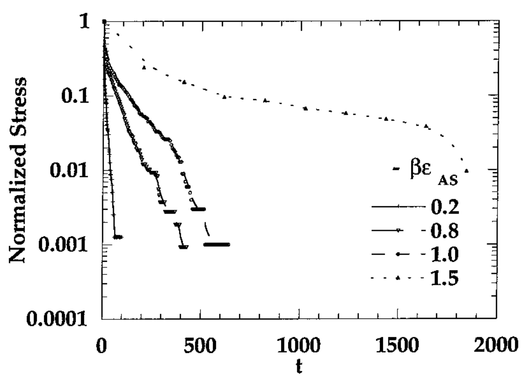

Figure 14. Normalized stress relaxation moduli for $N_B = 40$, $N_A = 5$, $D = 11$, and various values of $-\beta\epsilon_{AS}$.

energy at a given surface separation of $D = 11$ and $N_A = 5$. As expected, the relaxation behavior becomes increasingly more nonexponential and occurs on a slower time scale as the binding energy increases.

3.4. Complex Modulus: Storage and Loss Moduli. The dynamic mechanical behavior of viscoelastic materials can also be investigated using dynamic mechanical testing. Here, unlike in the stress relaxation measurements, a sinusoidal strain, i.e., $\gamma = \gamma' \sin \omega t$ (where ω is the angular frequency, radians per second), instead of a unit step strain is applied and the resulting stress is measured. In our analysis, we assume that ω is small such that the bridging lifetime distribution is not affected. The dynamic quantities obtained are the components of the dynamic modulus, the storage, $G'(\omega)$, and loss, $G''(\omega)$, moduli. The storage modulus, G', represents the energy stored elastically in the material during the straining. The energy that is lost by conversion to heat through molecular friction is represented by G''. The dynamic moduli, $G'(\omega)$ and $G''(\omega)$, respectively, are determined[22,32,33] from the relaxation modulus, $G(t)$, by the Fourier transforms:

$$G'(\omega) = \omega \int_0^\infty G(t) \sin \omega t \, dt \tag{5}$$

$$G''(\omega) = \omega \int_0^\infty G(t) \cos \omega t \, dt \tag{6}$$

and correspondingly the apparent stiffness of the material, $|G^*|$, where G^* is the complex modulus ($G^* = G' + iG''$), is calculated

$$|G^*| = (G'^2 + G''^2)^{1/2} \tag{7}$$

The high-frequency limit of $|G^*|$ and G' corresponds quantitatively to the stress relaxation modulus obtained in the short-time limit,

$$|G^*|(\omega \rightarrow \infty) = G'(\omega \rightarrow \infty) = G(t \rightarrow 0) \tag{8}$$

In panels a and b of Figure 15, the dynamic moduli are plotted versus ω for $N_A = 1$ and $-\beta\epsilon_{AS} = 1.0$ and 3.0, respectively. The frequency responses of the moduli are qualitatively similar to those of a Maxwell element, in agreement with our discussion in the previous section. The apparent stiffness, $|G^*|$, and the storage modulus increase to a limiting value with increasing frequency. The loss modulus passes through a maximum at an intermediate frequency. At low frequencies, the dashpot in the model offers little resistance to motion and thus not much energy is dissipated (low G''), while at high frequencies, its high resistance prevents its motion, and G'' falls off. The maximum in the loss modulus falls (also at the intersection of G' and G'') in the range of frequencies where the transition from the rubbery plateau to the flow region occurs. In the Maxwell model, the frequency at which the storage and loss moduli intersect corresponds to $2\pi/\tau_c$, where τ_c is the characteristic time.

In panels a and b of Figure 16, the effects of the binding energy on the storage and loss moduli, respectively, are depicted for $N_A = 1$. Panel a shows that the transition to the flow region is shifted to lower frequencies as the binding energy increases (or T decreases). Both the width and height of the plateau region increase as the binding energy increases. The loss modulus maximum is shifted to lower frequencies as the binding energy increases, as seen in panel b of Figure 16. In addition, as the binding energy increases, the peak broadens, becoming almost flat. These results have been qualitatively observed by Stadler and co-workers in their viscoelastic studies of transient networks from hydrogen-bonded polybutadiene.[25−28] The slope in the terminal zone (low frequencies) is approximately 2 in the log G' versus log ω plot and 1 in the log G'' versus log ω plot, typical numbers for melts of polymers with narrow molecular weight distribution.[32,33] These slopes do not appear to change as the binding energy increases.

The influences of the end block size on the storage and loss moduli are shown in panels a and b of Figure 17, respectively, for $-\beta\epsilon_{AS} = 0.4$. As illustrated in panel a, the height of the plateau region appears to decrease as N_A increases. The transition to flow region occurs at lower frequencies and the slope in the terminal zone decreases from 2.0 to ~1.0 as N_A increases from 1 to 15. In panel b of this figure the slope in the terminal zone decreases from 1.0 to ~0.5 as N_A increases from 1 to 15.

4. Conclusions

In this work, the equilibrium and dynamics properties of ABA triblock copolymer chains with adsorbing A

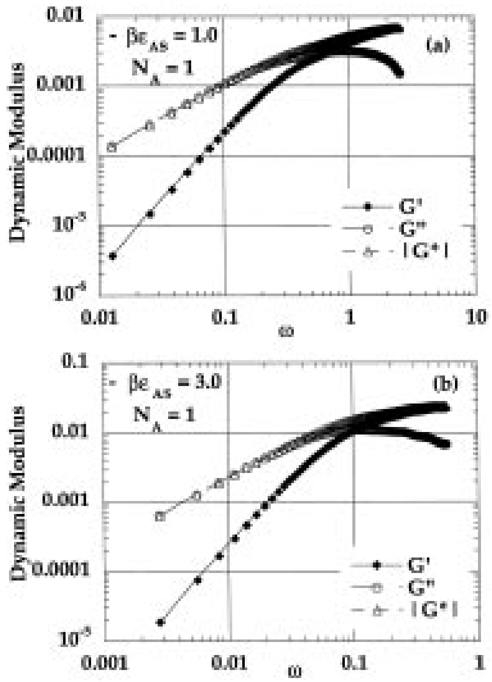

Figure 15. Frequency–response complex modulus for $-\beta\epsilon_{AS}$ of (a) 1.0 and (b) 3.0, with $N_A = 1$, $N_B = 40$, and $D = 11$.

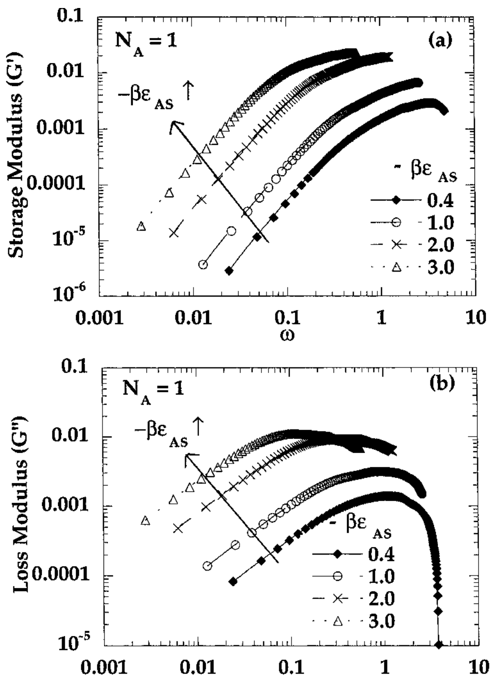

Figure 16. Effects of binding energy on (a) storage modulus and (b) loss modulus for $N_A = 1$, $N_B = 40$, and $D = 11$.

blocks confined between two parallel surfaces are determined in a concentration regime where there is little overlap between chains. The situation is similar to the unentangled network models and applicable to a suspension of colloidal particles with added triblock copolymers. As either $\beta\epsilon_{AS}$ or N_A increases, both the bridging and loop fractions increase, while the free fraction decreases and the dangling fraction passes through a maximum. The onset and degree of bridging determine the conditions of flocculation and the strength of the resulting network. In addition, the fraction of adsorbing A segments increases as either $\beta\epsilon_{AS}$ or N_A increases. Importantly, all these properties depend explicitly on N_A and ϵ_{AS}, not on the product $2\beta\epsilon_{AS}N_A$.

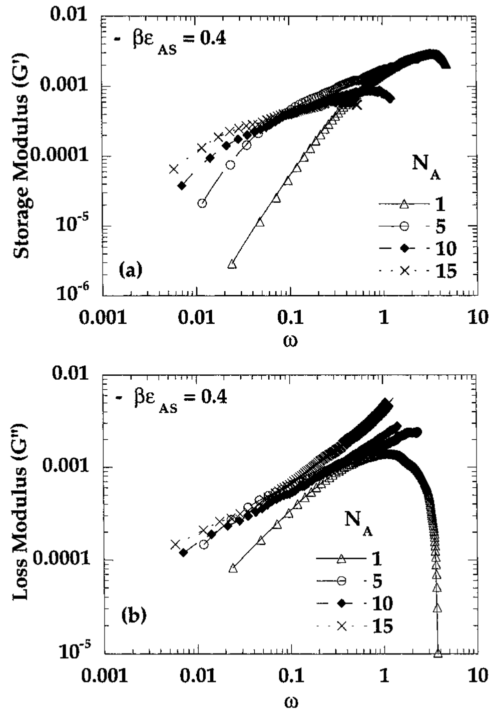

Figure 17. Effects of N_A on (a) storage modulus and (b) loss modulus for $-\beta\epsilon_{AS} = 0.4$, $N_B = 40$, and $D = 11$.

For a system of triblock copolymers with one A segment per end, the bridging lifetime distribution fits a single exponential function, leading to a stress decay that is also exponential. In contrast, for triblock copolymers with end block size that is greater than one, the lifetimes of bridges distributed nonexponentially, becoming increasingly more nonexponential as the end block gets longer. As a result, the stress relaxation response does not follow a simple exponential decay. We suggest that the response is a complex sum of several exponentials when more than one segment per A block is adsorbed. Furthermore, the dynamics of systems of triblock copolymer chains are controlled by the effective binding energy rather than the total available binding energy.

As the binding energy increases, the relaxation occurs on a slower time scale, similar to that of a system of triblock copolymers with one A segment per end block. The average bridging lifetime grows exponentially with the binding energy, regardless of the size of the A block. However, for triblock copolymer chains with $N_A = 1$, the relaxation characteristic time increases exponentially with the binding energy. As expected, for $N_A > 1$, although the relaxation characteristic time increases with the binding energy, the dependence is no longer exponential. The characteristic time also increases as the end block size increases. The plateau modulus, which increases with increasing binding energy, is independent of the end block size when $N_A > 5$. The average bridging lifetime and the characteristic relaxation time are rather insensitive to the separation of the surfaces up to a certain critical surface separation, after which they drop rapidly. The plateau modulus, however, decreases with increasing surface separation.

In response to a sinusoidal strain, the system with $N_A = 1$ exhibits a dynamic behavior that is characteristic of a Maxwell element. The plateau region in the log–log plot of the storage modulus versus ω broaden, as well as increase, in height as the binding energy increases. The transition to the flow region is shifted to lower frequencies as the binding energy increases (or T decreases). As the end block size increases from 1 to 15, the slope in the terminal zone decreases from 2 to 1 in the log G' versus log ω plot and decreases from 1 to 0.5 in the log G'' versus log ω plot, indicating slower relaxation for the larger end block size.

The strong influence of the adsorbing block size suggests that triblock copolymers could be tailored with relative ease to suitably modify the rheology of paints and other suspensions.

Acknowledgment. This research was supported by National Science Foundation Grant DMR 92-20369.

References and Notes

(1) Napper, D. H. *Polymeric Stabilization of Colloidal Dispersions*; Academic: New York, 1983.
(2) Granick, S.; Patel, S.; Tirrell, M. *J. Chem. Phys.* **1986**, *85*, 5370.
(3) Pelssers, E. G. M.; Cohen Stuart, M. A.; Fleers, G. J. *J. Chem. Soc., Faraday Trans.* **1990**, *86*, 1355.
(4) Dai, L.; Toprakcioglu, C. *Europhys. Lett.* **1991**, *16*, 331.
(5) Dai, L.; Toprakcioglu, C. *Macromolecules* **1992**, *25*, 6000.
(6) Watanabe, H.; Tirrell, M. *Macromolecules* **1993**, *26*, 6455.
(7) Johner, A.; Joanny, J.-F. *Europhys. Lett.* **1991**, *15*, 265.
(8) Milner, S. T.; Witten, T. A. *Macromolecules* **1992**, *25*, 5495.
(9) Wijmans, C. M.; Leermakers, F. A. M.; Fleer, G. J. *J. Colloid Interface Sci.* **1994**, *167*, 124.
(10) Misra, S.; Mattice, W. L. *Macromolecules* **1994**, *27*, 2058.
(11) Nguyen-Misra, M.; Mattice, W. L. *Macromolecules* **1995**, *28*, 1444.
(12) Green, M. S.; Tobolsky, A. V. *J. Chem. Phys.* **1945**, *14*, 80.
(13) Lodge, A. S. *Trans. Faraday Soc.* **1956**, *52*, 120.
(14) Yamamoto, M. *J. Phys. Soc. Jpn.* **1956**, *11*, 413.
(15) Tanaka, F.; Edwards, S. F. *J. Non-Newtonian Fluid Mech.* **1992**, *43*, 247.
(16) Tanaka, F.; Edwards, S. F. *J. Non-Newtonian Fluid Mech.* **1992**, *43*, 273.
(17) Tanaka, F.; Edwards, S. F. *J. Non-Newtonian Fluid Mech.* **1992**, *43*, 289.
(18) Tanaka, F.; Edwards, S. F. *Macromolecules* **1992**, *25*, 1516.
(19) Wang, S.-Q. *Macromolecules* **1992**, *25*, 7003.
(20) Baxandall, L. G. *Macromolecules* **1989**, *22*, 1982.
(21) Gonzalez, A. E. *Polymer* **1983**, *24*, 77.
(22) Gonzalez, A. E. *Polymer* **1984**, *25*, 1469.
(23) Leibler, L.; Rubinstein, M.; Colby, R. H. *Macromolecules* **1991**, *24*, 4701.
(24) Graessley, W. W. *Adv. Polym. Sci.* **1982**, *47*, 67.
(25) Stadler, R.; de Lucca Freitas, L. L. *Colloid Polym. Sci.* **1986**, *264*, 773.
(26) de Lucca Freitas, L. L.; Stadler, R. *Macromolecules* **1987**, *20*, 2478.
(27) Stadler, R. *Prog. Colloid Polym. Sci.* **1987**, *75*, 140.
(28) Stadler, R.; de Lucca Freitas, L. L. *Macromolecules* **1989**, *22*, 714.
(29) Misra, S.; Nguyen-Misra, M.; Mattice, W. L. *Macromolecules* **1994**, *27*, 5037.
(30) Bevington, P. R. *Data Reduction and Error Analysis for the Physical Sciences*; McGraw-Hill: New York, 1969.
(31) Annable, T.; Buscall, R.; Ettelaie, R.; Whittlestone, D. *J. Rheol.* **1993**, *37*, 695.
(32) Rosen, S. L. *Fundamental Principles of Polymeric Materials*; John Wiley & Sons: New York, 1982.
(33) Ferry, J. D. *Viscoelastic Properties of Polymers*, 3rd ed.; Wiley: New York, 1980.

MA950802S